Intramolecular Dynamics and Unimolecular Decomposition of Polyatomic Molecules in Rare-Gas Clusters: Cluster Size Effects in H_2O_2–Ar_N (N = 1–39)

Lisa M. Finney and Craig C. Martens*

Department of Chemistry, University of California, Irvine, Irvine, California 92717-2025

Received: August 2, 1993®

The cluster size and structure dependence of local microsolvation environment on intramolecular energy transfer and unimolecular dissociation is studied for the systems H_2O_2–Ar_N (N = 1–39) using the method of classical trajectory simulation. The rates and mechanisms of intramolecular energy transfer and molecular decomposition of the complex are investigated as a function of N. Three major mechanisms for cluster modification of isolated molecule behavior are operative: vibrational deactivation of the excited molecule, modification of intramolecular energy redistribution, and cluster-induced recombination. The evolution of these effects is studied as cluster size and structure are varied. It is found that the degree of solvation of the hydrogen peroxide molecule, rather than the absolute cluster size, determines the extent of the cluster effects.

I. Introduction

The properties of weakly-bound clusters are currently the focus of considerable experimental and theoretical interest.[1-9] Finite clusters constitute a novel state of matter which is, in some sense, intermediate between isolated few-body systems and true condensed phases. Dynamical processes in clusters provide models of solvation,[10-21] solvent caging,[10,22-32] phase transitions,[33-47] diffusion,[13,48-51] chemical reactions[10,13-16,22,23,26,52-67] and other condensed-phase processes in well-defined systems where the rigorous methods of gas-phase chemical physics can be applied. By systematic variation of the size of clusters in an experiment or simulation, the evolution of behavior from the limits of small complexes to the condensed phase can be investigated.

In this paper, we study the cluster size dependence of the intramolecular energy redistribution and unimolecular decomposition dynamics of a polyatomic molecule associated with a rare-gas cluster. The particular systems considered are H_2O_2–Ar_N, for N = 1–39. We apply the method of classical trajectory simulation to model the dynamics following overtone excitation of an OH stretch for a series of cluster sizes and compare the results with analogous calculations on the isolated molecule. In a previous publication,[53] we described the dynamics of the particular case of H_2O_2–Ar_{13}. Here, we extend that study and investigate the dependence of the rates and dynamical mechanisms of intramolecular energy redistribution and unimolecular dissociation on the size and structure of the Ar solvent cluster.

Size effects in clusters have been the focus of a wide range of experimental and theoretical investigations.[1-9,68-70] These studies have addressed a number of aspects of the chemistry and physics of finite cluster systems, including the emergence of bulk structure with increasing size,[71-74] the size dependence of electronic structure,[3] the role of quantum effects,[2,3,68] finite-size thermodynamics,[34,35,38,75,76] and influence of size and structure on cluster spectroscopy[12,77,78] and dynamics.[69,70,79] Issues such as cluster rigidity, isomerization, and finite system analogues of phase transitions have also been addressed.[34,69]

The size dependence of molecular dynamics in highly excited clusters has been the focus of a number of experimental and theoretical studies. Amar and Berne investigated the role of solvent caging on photodissociation and recombination in molecular dynamics simulations of the Br_2–Ar_N systems (N = 8–70).[23] Theoretical studies of the photodissociation dynamics of Br_2^- in Ar and CO_2 clusters of varying size have been reported;[80] this work was motivated by mass-resolved experiments performed on Br_2^- in CO_2 clusters by the Lineberger group.[22] Photofragmentation studies of I_2^- in small $(CO_2)_N$ clusters (N = 0–22) by Lineberger and co-workers have focused on the effect of cluster size on photodissociation and recombinant dynamics.[29,30] Monte Carlo calculations by the same group[29] and molecular dynamics simulations by Amar and Perera on $I_2^-(CO_2)_N$[81] have provided a theoretical perspective of size-dependent caging effects in clusters. Molecular dynamics simulations by Perera and Amar involving small molecules associated with van der Waals clusters have addressed the dependence of spectral shifts on cluster size and structure;[82] these theoretical studies were motivated by infrared spectroscopic investigations of Scoles and co-workers of molecules in Ar clusters.[12,77,83-86]

In ref 53 we presented a computational study of the dynamics of overtone-induced unimolecular decomposition of hydrogen peroxide associated with an Ar_{13} cluster. We identified three major effects of cluster solvation on the dynamics of the H_2O_2 molecule: (i) vibrational deactivation of the excited molecule via both molecule to cluster energy relaxation and cluster-mediated intramolecular vibration–rotation energy transfer, (ii) cluster modification of intramolecular vibrational energy redistribution, and (iii) cluster-induced recombination of the OH fragments.

In the present study, we examined the evolution of these effects with both the size and the structure of the Ar_N cluster microsolvation environment. Classical trajectory methods, combined with strictly classical initial conditions, are employed to model the dynamics. Cluster sizes with N = 1–39 are considered, and the results are compared with those of the isolated molecule. For geometries with the H_2O_2 molecule in a highly solvated site (i.e., "inside" of the cluster), we investigate the dependence of dynamical rates and mechanisms of the number of cluster atoms. For a fixed N = 13, we assess the effects of changing the geometric structure of the cluster, comparing H_2O_2 at the center of the cluster with H_2O_2 in a cluster surface site. The size and structure dependences of the recombination probability are also investigated. As described below, we find that it is the degree of solvation of the molecule by the cluster atoms, rather than the absolute size of the cluster, that determines the extent of the dynamical effects of microsolvation.

The dynamics of isolated H_2O_2 in the gas phase has been the subject of recent experimental[87-94] and theoretical[95-102] studies. We also note recent and related work on overtone-induced decomposition of HOCl in Ar gas and liquid reported by Li *et al.*[103]

The organization of the rest of this paper is as follows: In

* To whom correspondence should be addressed.

® Abstract published in *Advance ACS Abstracts*, November 15, 1993.

0022-3654/93/2097-13477$04.00/0

section II, the classical trajectory method used to simulate the dynamics of H_2O_2–Ar_N is described, and the potential energy surface employed in this study is presented. In addition, the methodology used to find energy minimum structures, generate initial conditions, integrate classical trajectories, and analyze the resulting data is described. The results of the simulations are presented in section III, along with a discussion of the observed size- and structure-dependent trends in the dynamical behavior. Finally, a summary is given in section IV.

II. Method

The dynamics of isolated H_2O_2 and the molecule–cluster complexes H_2O_2–Ar_N are modeled by classical trajectory simulation. In this section, we describe the potential energy surface and outline the methods employed to generate minimum energy geometries and trajectory ensemble initial conditions. In addition, we outline our analysis of the resulting simulation data.

(A) Potential Surface. The potential energy surface of the H_2O_2–Ar_N system used in this study is of the general form

$$V = V_m + V_c + V_{m-c} \tag{1}$$

The first term, V_m, is the intramolecular potential energy surface of the isolated hydrogen peroxide molecule, while V_c and V_{m-c} are Ar–Ar and Ar–H_2O_2 interactions, respectively. For V_m, we adopt the potential surface developed by Getino *et al.*, which is based on a fit to *ab initio* calculations.[102] The intramolecular potential consists of three terms:

$$V_m = V_{stretch} + V_{bend} + V_{torsion} \tag{2}$$

corresponding to two-body stretches, three-body bends, and four-body torsional interactions, respectively. The two-body stretch potential is modeled by a sum of Morse oscillators:

$$V_{stretch} = \sum_{i=1}^{3} D_i(1 - e^{-\beta_i(r_i - r_i^e)})^2 \tag{3}$$

where D_i are the bond dissociation energies, and β_i are scale factors. The r_i and r_i^e are instantaneous and equilibrium bond distances, respectively. The three-body term corresponds to the OOH bend degrees of freedom and is given as the sum of harmonic interactions, each with a force constant k:

$$V_{bend} = \sum_{i=1}^{2} S_i(r_i)S_{i+1}(r_{i+1})(k/2)(\theta_i - \theta_i^e)^2 \tag{4}$$

Here θ_i and θ_i^e are the instantaneous and equilibrium bend angles, respectively. The force constants are attenuated by switching functions $S(r)$, which we describe below. The four-body torsion is represented as a trigonometric series:

$$V_{torsion} = S_1(r_1)\, S_2(r_2)\, S_3(r_3) \sum_{m=0}^{3} A_m \cos^m(\phi) \tag{5}$$

where ϕ is the torsion angle, and A_m are constant Fourier components. The torsional potential is also modified by switching functions.

Switching functions are used to model the attenuation of the bend and torsional interaction strengths with OH and OO bond lengths. The switching function used for the OH bonds is given by

$$S_i(r_i) = \begin{cases} 1 & r_i \le r_i^e \\ \exp[-B(r_i - r_i^e)^2] & r_i > r_i^e \end{cases} \tag{6}$$

The corresponding OO bond switching function is taken to be

$$S_i(r_i) = 1 - \tanh[C(r_i - r_i^e)^5] \tag{7}$$

These switching functions were determined from fits of *ab initio* calculations for the isolated molecule.[102] The parameters used in V_m are listed in Table III, and the resulting normal-mode frequencies are given in Table II. See refs 53 and 102 for further details of the intramolecular potential function.

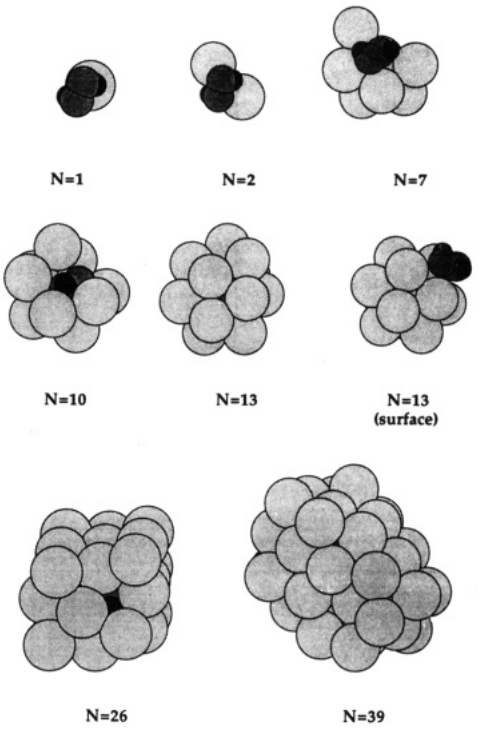

Figure 1. Minimum geometry structures of H_2O_2–Ar_N clusters.

TABLE I: Local Minima Energies

system	energy (cm^{-1})
H_2O_2–Ar	–157.21
H_2O_2–Ar_2	–383.54
H_2O_2–Ar_7	–1958.93
H_2O_2–Ar_{10}	–2985.73
H_2O_2–Ar_{13}	–4284.14
H_2O_2–Ar_{26}	–9290.40
H_2O_2–Ar_{39}	–15261.86
H_2O_2–Ar_{13} (surface)	–4151.84

The cluster interactions, V_c and V_{m-c}, are modeled by pairwise additive potentials. Each atom–atom interaction is taken to be a Lennard-Jones potential function:

$$V_c = \sum_{i=1}^{N_c-1} \sum_{j=i+1}^{N_c} 4\epsilon_c[(\sigma_c/r_{ij})^{12} - (\sigma_c/r_{ij})^6] \tag{8}$$

$$V_{m-c} = \sum_{i=1}^{N_m} \sum_{j=1}^{N_c} 4\epsilon_{ij}[(\sigma_{ij}/r_{ij})^{12} - (\sigma_{ij}/r_{ij})^6] \tag{9}$$

where ϵ_c, ϵ_{ij}, σ_c, and σ_{ij} are the appropriate Lennard-Jones parameters. N_c and N_m are the number of cluster and molecule atoms, respectively. See Table III for numerical values of the potential parameters.

(B) Cluster Geometries. Local minimum energy structures for each cluster size were found by kinetic energy quenches of high energy trajectories, which were started from estimated initial geometries. Several heating and cooling cycles were performed in an attempt to find the structures corresponding to global energy minima. The lowest energy geometries found for each molecule–cluster system are illustrated in Figure 1, and the energies corresponding to these structures are given in Table I. The low-energy structures for clusters with 13 or more Ar atoms are characterized by a complete "solvation shell" surrounding the H_2O_2 molecule. Other local minima, with the hydrogen peroxide

TABLE II: Normal-Mode Frequencies[a]

mode	ω (cm^{-1})
OH sym	3883
OH str	3882
OOH sym bend	1474
OOH asym bend	1402
torsion	406

[a] Normal-mode frequencies of hydrogen peroxide potential, eq 2.

TABLE III: Potential Parameters

D_{OH}	88.6 kcal/mol	A_2	3.206 kcal/mol
r^e_{OH}	0.965 Å	A_3	−0.488 kcal/mol
β_{OH}	2.62 Å^{-1}	ϵ_{Ar-Ar}	0.0638 kcal/mol
D_{OO}	49.6 kcal/mol	σ_{Ar-Ar}	3.410 Å
r^e_{OO}	1.452 Å	ϵ_{O-Ar}	0.1706 kcal/mol
β_{OO}	2.58 Å^{-1}	σ_{O-Ar}	3.180 Å
θ^e	1.745 rad	ϵ_{H-Ar}	0.2379 kcal/mol
k	0.99 mdyn Å/rad^2	σ_{H-Ar}	3.110 Å
A_0	0.865 kcal/mol	C	0.1205 Å^{-5}
A_1	3.453 kcal/mol	B	1.58 Å^{-2}

"adsorbed" on the surface of the cluster, were found for the larger systems. However, these surface structures are higher in energy than their highly solvated isomers. For general N, we considered only the lowest energy structure. Calculations were performed using both the lower energy "caged" structure and the higher energy "adsorbed" geometry for H_2O_2–Ar_{13}. The structure of the $N = 13$ surface site cluster is also shown in Figure 1, and its energy is included in Table I.

(C) Initial Conditions. The minimum energy geometries described above were used to generate ensembles of initial conditions for the trajectory calculations. For a given configuration, each atom of the system was assigned a random velocity from a Maxwellian distribution corresponding to a system temperature of 10 K. The velocities were then adjusted to yield zero total linear and angular momenta. The ensemble of initial conditions was then propagated for 120 ps, with periodic rescaling of the velocities to correct the time-averaged kinetic energy to yield the desired initial temperature of 10 K. For a given N, ensembles of 200–300 trajectories were generated by repeating this process for each trajectory, starting with different initial random velocities.

The thermal ensemble was then subjected to overtone excitation of an OH local mode vibration. This was accomplished by adjusting the OH bond momentum of one OH stretch, chosen randomly, to yield a classical energy corresponding to the desired vibrational quantum number v. The positions and momenta of all atoms were then stored and used as initial conditions for the trajectory simulations.

The initial conditions employed in this study are purely classical, in that they do not take into account zero-point energy in the vibrational modes of the cluster or molecule. This is necessary to avoid spurious dynamical processes, which can be induced by redistribution of the classical zero-point energy. For a given initial overtone excitation, the absence zero-point energy in the other vibrational modes results in a molecule with total energy significantly less than the case where it is included. Thus, the unimolecular rate calculated here will be less, for a given v, than the result of calculations performed on the same potential surface which include the zero-point energy. Classical trajectory calculations performed on this surface with zero point energy included are reported in ref 102 and are in general qualitative agreement with experiment. We have chosen to neglect zero-point energy and treat all processes as purely classical. Consequently, this system must be viewed as a model problem and is not meant to be a realistic representation of the quantum dynamics of a hydrogen peroxide molecule.

(D) Classical Trajectory Integration. Ensembles of classical trajectories were propagated for 33 ps by numberical integration of Hamilton's equations. A sixth-order hybrid Gear routine[104] was employed for the numerical integrations. The accuracy of these long integrations was monitored by energy conservation, as well as by conservation of the total linear and angular momenta. Errors in the total energy were approximately 1 part in 10 000.

(E) Trajectory Data Analysis. The ensemble-averaged energy transfer within the cluster–molecule system was monitored as a function of time. The total energy was separated into molecule, cluster, and molecule–cluster interaction contributions. The energy of the H_2O_2 molecule was partitioned into vibrational, rotational, and translational energies, and the vibrational energy was further divided (approximately) into the six internal modes using the method of Wilson, as described in ref 102. The dynamiical G matrix was calculated as a function of time, and the diagonal elements used along with the single-mode potential functions to calculate the mode energies:

$$E_j(t) = G_{jj}[\mathbf{r}(t)]p_j(t)^2 + V_j[\mathbf{r}(t)] \qquad (10)$$

where $\mathbf{r}(t)$ and $\mathbf{p}(t)$ are the instantaneous values of the internal coordinates and conjugate momenta, respectively, and V_j is the term in the potential corresponding to mode j. For the bend and torsion, the stretch-dependent switching functions are included in the definition of V_j. This method neglects the kinetic cross terms coupling the internal degrees of freedom, which make a relatively small contribution to the vibrational energy, especially after ensemble averaging is performed. The time histories of these energies were stored for each member of the ensemble, in addition to their ensemble-averaged values.

The unimolecular decomposition times were determined for each trajectory by monitoring the OO bond distance as a function of time and using a critical extension as a condition for dissociation. The actual time of dissociation was taken to be the time of the previous inner turning point of the OO bond. We also employed an energy criterion, where dissociation was taken as the time when the OO bond energy exceeded D_{OO}. Recombination was assumed to have occurred when this mode energy dropped back below D_{OO}. Both methods gave equivalent results for dissociation. The energy criterion was more convenient for detecting recombination events.

III. Results and Discussion

In this section, we describe the results of trajectory calculations of H_2O_2–Ar_N dynamics for several N, and for two levels of initial OH vibrational excitation: $v = 5$ and $v = 7$. For $v = 5$, dissociation cannot occur for our system, while decomposition is energetically possible for $v = 7$. The results obtained for molecule–argon cluster complexes are compared with those for the isolated molecule using analogous classical initial conditions.

The smallest cluster system studied consists of the H_2O_2 molecule bound to a single Ar atom, while the largest system is H_2O_2–Ar_{39}. Several intermediate N are also considered, so that the complete study treats $N = 1$, 2, 7, 10, 13, 26, and 39. The isolated system is also treated for comparison. For the $N = 13$ system, two geometries are considered: a cluster with the molecule highly solvated by the cluster atoms, and a distinct (higher energy) geometry with the molecule on the surface of the cluster. The structures of these systems are displayed in Figure 1.

In a previous study,[53] we investigated the dynamics of the $N = 13$ system. Three important dynamical mechanisms affecting the overall behavior were identified: (i) vibrational deactivation of the excited molecule, (ii) cluster modification of intramolecular energy-transfer dynamics, and (iii) cluster-induced recombination of nascent OH fragments. In the present work, we examine the dependence of these processes on both the size and the initial geometry of the cluster–molecule complex.

Vibrational Deactivation. In ref 53, it was observed that the Ar cluster induces vibrational energy relaxation of the hydrogen peroxide molecule in H_2O_2–Ar_{13}, which can lead to deactivation of potentially dissociative trajectories. The vibrational deacti-

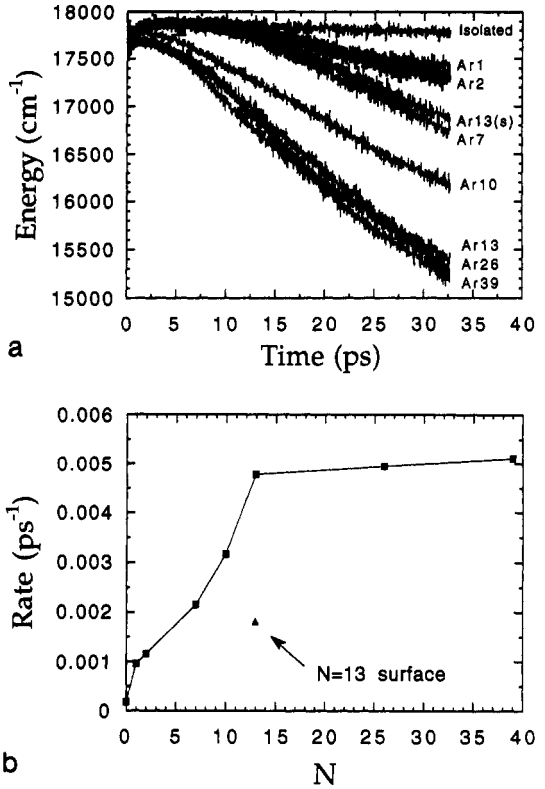

Figure 2. Vibrational deactivation of hydrogen peroxide by the argon cluster. The curves shown are ensemble averaged vibrational energies of H_2O_2 embedded in clusters Ar_1, Ar_2, Ar_7, Ar_{10}, Ar_{13}, Ar_{26}, Ar_{39} for $v = 5$. Also plotted is the ensemble averaged vibrational energy of H_2O_2 adsorbed to the surface of an Ar_{13} cluster.

vation was found to occur by two mechanisms: (i) molecule–cluster energy transfer in the form of vibrational and rotational relaxation and (ii) cluster "catalyzed" energy flow from internal vibration to molecular rotation. Here, we investigate the dependence of vibrational energy relaxation on the size and structure of the cluster. For this portion of the study, we consider ensembles with initial OH excitation of $v = 5$; the resulting energy is below the dissociation threshold of our model.

In Figure 2, we show results for the vibrational energy relaxation of the isolated molecule and the $N = 1$, 2, 7, 10, 13, 26, and 39 highly solvated geometries. In addition, the $N = 13$ surface geometry data is displayed [labeled $Ar_{13}(s)$]. Figure 2 (a) gives a composite plot of the vibrational energies of each ensemble vs time. The total vibrational energy of H_2O_2 was approximated by the sum of the internal mode energies, as given in eq 10, and averaged over each ensemble. Figure 2b shows the vibrational relaxation rate of each ensemble as a function of N, determined by fitting the logarithm of the data shown in Figure 2a for times between 10 and 25 ps; the decay was reasonably well-represented by an exponential in this time range for all ensembles.

Figure 2 demonstrates that the rate of vibrational energy deactivation depends on both the size and the structure of the cluster. For the highly solvated series, the vibrational relaxation rate increases monotonically with cluster size. The isolated molecule has a conserved vibrational energy. Adding a single Ar atom to the system causes slow energy flow out of the vibrational degrees of freedom. Additional cluster atoms lead to increases in the rate of vibrational deactivation. The largest changes in behavior occur as the first solvation shell around the H_2O_2 molecule is built up and completed at $N = 13$. For $N > 13$, the addition of atoms to the cluster leads to only small changes in the relaxation behavior.

The $N = 13$ surface site ensemble exhibits a vibrational relaxation rate that is slightly less than the $N = 7$ ensemble. Inspection of Figure 1 shows that the extent of H_2O_2 solvation is similar in these two cases and demonstrates that the structure of the molecule solvation environment is the most important characteristic of the system influencing the vibrational relaxation dynamics, rather than the absolute size of the cluster.

Cluster Modification of Intramolecular Vibrational Energy Transfer. In ref 53, we described the effect of cluster solvation on the intramolecular vibrational energy redistribution (IVR) dynamics of H_2O_2–Ar_{13}. Here we investigate the influence of cluster size and structure on IVR. We again consider the $v = 5$ ensemble, to avoid the competing process of unimolecular decomposition.

In parts a–d of Figure 3 we show the ensemble-averaged mode energies for the isolated molecule and the $N = 1$, $N = 7$, and $N = 13$ ensembles, respectively. The data are labeled as follows: OH1 is the energy of the initially excited OH stretch; OH2 is the energy of the OH stretch that is unexcited initially; B1 is the energy of the bend adjacent to the initially excited OH stretch; B2 is the energy of the distant OOH bend; OO is the energy of the OO bond, and TOR is the torsional energy. These quantities were evaluated by averaging the energies of each mode over the trajectory ensemble. Mode energies were evaluated as described in section II.E.

For each ensemble, the OH1 initial energy is approximately 17 700 cm^{-1}. The scale of the plot has been chosen to emphasize lower energies, so the initial OH1 excitation is off-scale. Following initial excitation, the excited OH stretch relaxes into the other modes of the molecule. It should be noted that equipartition of the energy is not complete by the end of the 33-ps integration.

As the size of the cluster increases, the behavior of the molecular mode energies evolves from the isolated dynamics shown in Figure 3a to the dynamics of the completely solvated molecule, given in Figure 3d. For larger cluster sizes (not shown), the results are similar to those for the $N = 13$ ensemble. A number of size-dependent trends can be observed. First, the OH1 relaxation rate increases with increased solvation. The initial step of OH stretch relaxation is energy transfer into the bend, and this can be promoted by collisions between the vibrating H atom and the solvent Ar atoms when the cluster is present. A second effect is inhibition of energy flow into the internal rotation of the molecule as the cluster size increases. Although this low-frequency mode does not couple strongly to the higher frequency stretches and bends, causing energy transfer into TOR to lag behind that into other modes, nearly 1000 cm^{-1} of torsional excitation is present on average at the end of the 33-ps simulation for the isolated H_2O_2 ensemble. As the solvation of the molecule is built up, the increased intermolecular interactions inhibit internal rotation, leading to less than 200 cm^{-1} of energy in TOR for the $N = 13$ ensemble at 33 ps.

The cluster effect on torsional motion is further illustrated in Figure 4. Here, the ensemble-averaged torsional energy vs time is presented for each of the ensembles. For the highly solvated geometries, the extent of energy flow into TOR decreases monotonically with cluster size. The ensemble with hydrogen peroxide on the surface of an $N = 13$ cluster shows behavior that is quite similar to the $N = 7$ ensemble. Again, this results from the similar local solvation environment of H_2O_2 in the two cases.

The most significant modification of IVR dynamics involves the extent of energy equipartition between the bends and the OO stretch. For the isolated molecule ensemble, shown in Figure 3a, the energies of the B1, B2, and OO subsystem have equilibrated by the end of the simulation. The initial energy relaxation step is transfer from OH1 into B1. The two bend modes can rapidly exchange energy, and the rises of the B1 and B2 energies seen in Figure 3a are very similar. The energy transfer into the OO stretch is somewhat slower than bend–bend exchange, leading to a lag in the OO energy. By approximately $t = 20$ ps, however, nearly complete redistribution of available energy has occurred between B1, B2, and OO.

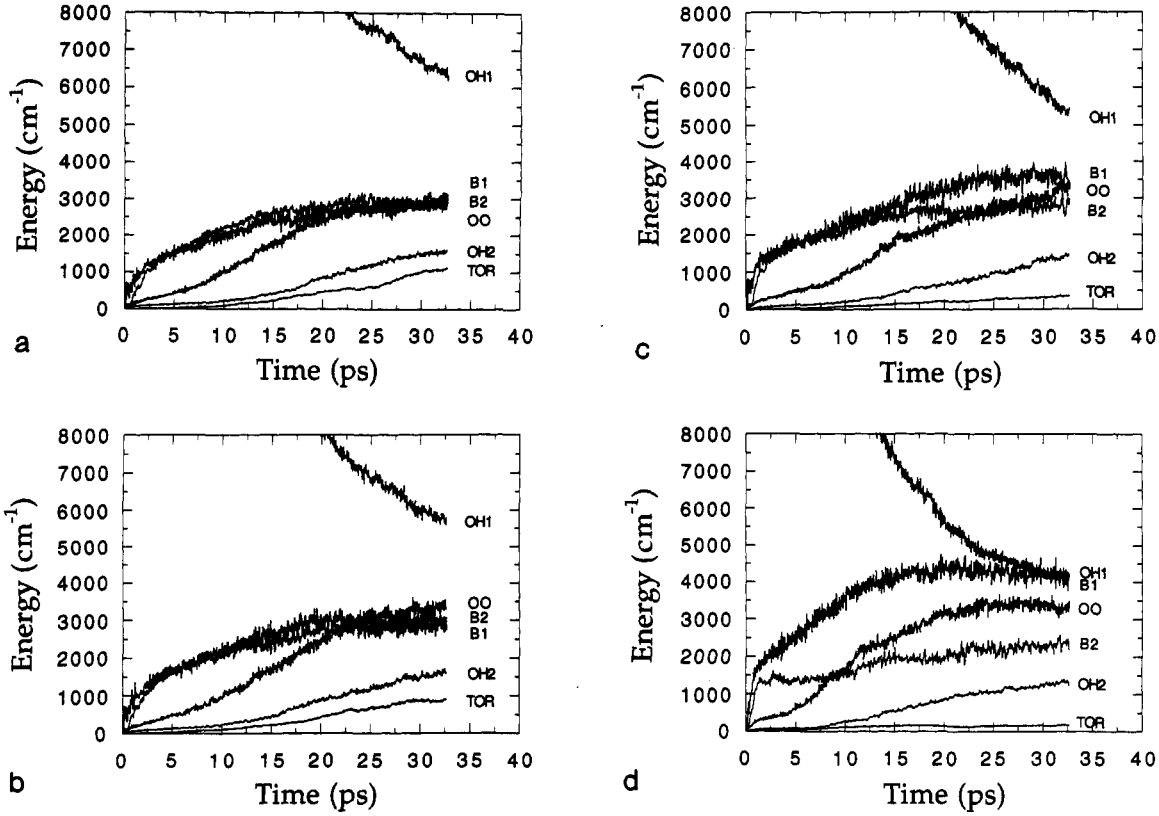

Figure 3. Ensemble-averaged mode energies for (a) isolated H_2O_2 and H_2O_2 associated with (b) Ar_1, (c) Ar_7, and (d) Ar_{13}. Each ensemble has an initial OH excitation corresponding to $v = 5$. The labeling is as follows: OH1 is the initially excited OH bond energy, OH2 is the other OH bond energy, B1 is the energy of the bend mode adjacent to the initially excited OH stretch, B2 is the energy of the distant bend, and TOR is the torsional energy. The vertical position of these labels indicate the ordering of the magnitudes of the mode energies.

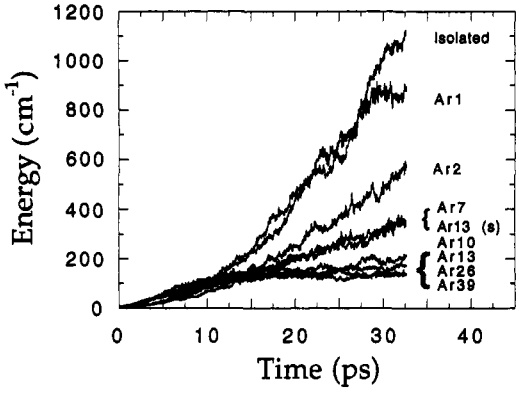

Figure 4. Ensemble-averaged torsional (TOR) energies of the H_2O_2–Ar_N systems with initial excitation corresponding to $v = 5$. The size and structure of the Ar clusters are labeled.

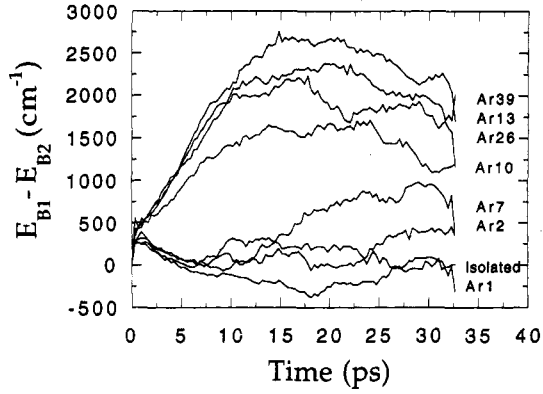

Figure 5. Difference between the two ensemble averaged bend energies ($E_{B1} - E_{B2}$) for the molecule–cluster complexes with initial excitation corresponding to $v = 5$, for all the value of N considered.

As solvent atoms are added to the system, the character of the (B1, B2, OO) subsystem changes. Increased solvation of the molecule leads to a breakdown of complete energy equilibration between these modes. For $N = 1$, the dynamics closely resemble the isolated molecule case. As the size of the cluster increases to $N = 7$, however, it is found that the energies of B1 and B2 have not equilibrated by the end of the simulation. The difference in bend energies becomes even more pronounced for the $N = 13$ results shown in Figure 3d. Here, the bend adjacent to the initially excited OH stretch, B1, has nearly twice the energy of the distant bend at $t = 33$ ps. The OO energy of the ensemble is approximately the average of B1 and B2 energies.

In Figure 5 we examine systematically the "disequilibrium" of bend energies as a function of cluster size and structure. Here, we show a composite plot of $E_{B1} - E_{B2}$ vs time for all ensembles considered. At early times, all ensembles show a short-time positive value for this quantity, as energy is transferred from OH1 into B1. This transient quickly decays as the bends exchange energy for the isolated, $N = 2$, $N = 7$, and $N = 13$ (surface) ensembles, which are characterized by incomplete solvation of the H_2O_2 molecule. As the first solvation shell becomes nearly complete for $N = 10$, a transition in behavior occurs, with the initial disequilibrium of bend energies persisting at longer times. The behavior of the ensembles with complete first solvation shells ($N = 13$, 26, and 39) are all similar, with a positive deviation of bend energies of roughly 2000 cm^{-1} existing at the end of the simulation.

The cluster environment is clearly affecting the intramolecular dynamics of hydrogen peroxide. As the degree of solvation by cluster atoms increases, large-amplitude molecular vibrations become increasingly inhibited by molecule–cluster repulsive interactions. Both torsional excitation and facile bend–bend energy transfer are suppressed by the presence of the associated Ar cluster.

Unimolecular Dissociation and Recombination. We now consider ensembles of trajectories with initial OH excitation

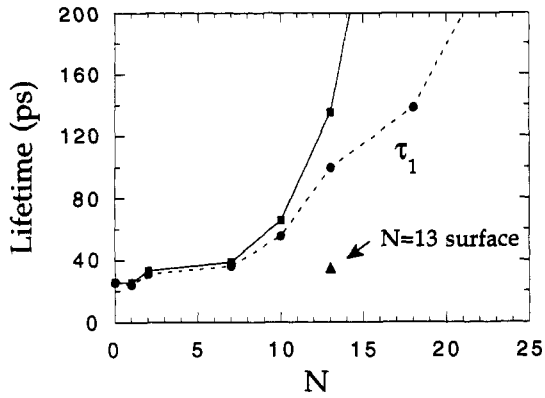

Figure 6. Unimolecular lifetime of H_2O_2 as a function of cluster size and structure, for an initial OH excitation of $v = 7$. See the text for further details.

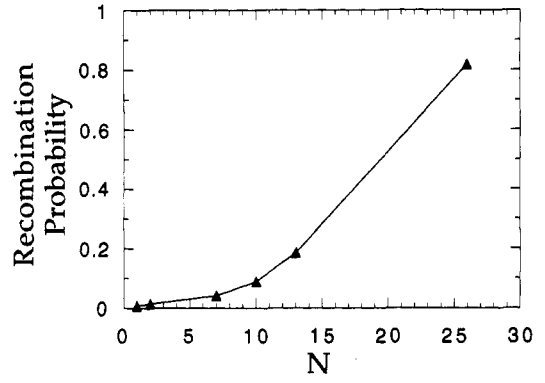

Figure 7. Cluster size dependence of recombination probability for molecules with an initial OH excitation of $v = 7$.

corresponding to $v = 7$. In this case, the molecules contain enough energy to undergo unimolecular dissociation. For the isolated molecule with classical initial conditions (i.e., no zero-point energy added to the vibrational degrees of freedom), this level of excitation results in a unimolecular lifetime of approximately 26 ps.[53] As cluster atoms are added to the system, the unimolecular kinetics and dynamics are modified, altering the lifetime of the overtone excited hydrogen peroxide molecule.

The dependence of the unimolecular lifetime of $H_2O_2(v=7)$ on cluster size is shown as the solid curve in Figure 6. The lifetime increases with N gradually from the isolated molecule value until $N = 7$. Beyond this cluster size, the lifetime lengthens dramatically, becoming too long to determine from our simulations for $N > 13$. The slowing of the dissociation rate with N is due to a combination of effects: vibrational deactivation, modified IVR, and recombination events. A detailed discussion of these processes for the case of $N = 13$ was given in ref 53.

One effect of the cluster on the unimolecular decomposition of H_2O_2 is its ability to cause recombination of the nascent OH radicals. The atoms of the cluster provide a channel for translational and rotational energy relaxation of the decomposition products and exert attractive van der Waals forces which can bind the fragments to the surface of the parent cluster. Both of these processes become more effective as the degree of solvation of the initial molecule is increased, and recombination is a major component of the increasing lifetime with cluster size. Figure 7 shows the probability of recombination as a function of N for the $v = 7$ ensembles. The recombination probability increases with increasing cluster size and is approximately 80% for H_2O_2–Ar_{26}.

The solid curve of Figure 6 is based on the kinetics of the decay of the total number of intact hydrogen peroxide molecules with time. If recombination events can occur, the effective lifetime of the molecule is lengthened. To investigate the size dependence of the cluster on unimolecular decomposition *beyond* the effect of recombination, we calculated an alternative lifetime which characterizes the decomposition of H_2O_2 *irrespective* of whether later recombination occurs or not. For the determination of this quantity, shown as a dashed curve labeled τ_1 on Figure 6, a molecule is removed from the ensemble once it undergoes its initial decomposition. This lifetime thus is not influenced by subsequent recombination. The growing difference between these two types of lifetimes with N indicates the increasing dominance of recombination in the unimolecular decomposition dynamics of the peroxide molecule with cluster size.

Also shown in Figure 6 are the data for H_2O_2–Ar_{13} in the surface site geometry. Again, the behavior of this adsorbed geometry shows less deviation from the isolated molecule case than the highly solvated $N = 13$ (surface) ensemble and is close in behavior to the $N = 7$ case, where the local microsolvation structure is similar.

IV. Summary

In this paper, we have presented a systematic study of the size and structure dependence of intramolecular energy transfer and unimolecular decomposition of H_2O_2–Ar_N following initial OH overtone excitation. This work extends the study reported in ref 53, where the single case of $N = 13$ was investigated, to consider the evolution of dynamical behavior with the number of Ar atoms and structural variations of the local microsolvation environment of the H_2O_2 molecule. Three major processes have been explored: (i) vibrational deactivation of the initially excited molecule, (ii) modification of the rate and extent of intramolecular energy transfer, and (iii) cluster-induced recombination of nascent OH fragments, and the effect of these processes on the H_2O_2 unimolecular dissociation dynamics has been characterized as a function of cluster size and structure.

For a series of clusters with minimum energy geometries corresponding to the H_2O_2 in a highly solvated site, the effects of the cluster become more pronounced with size, and show the most dramatic changes as the first solvation shell around the H_2O_2 is completed. For a fixed cluster size, the magnitude of the cluster's influence depends on the *degree* of solvation, with a highly solvated molecule showing much greater modification of its behavior than a molecule on the surface of a cluster of the same size. From the perspective of observable rates of reactions, the major effect of the cluster is a lengthening of the lifetime with increasing solvation of H_2O_2 by argon atoms.

The particular systems considered here illustrate the general evolution of solvent effects on IVR and unimolecular reaction, from the isolated molecule limit, through small complexes of a few components, and finally to relatively large clustes containing tens of atoms. The study thus provides a bridge between previous contributions on chemical dynamics in isolated molecules[95-102] and investigations of dynamical processes in the condensed phase.[103]

References and Notes

(1) *The Physics and Chemistry of Small Clusters*; Jena, P., Rao, B. K., Khanna, N., Eds.; Plenum: New York, 1986.
(2) *The Chemical Physics of Atomic and Molecular Clusters—Proceedings of the Enrico Fermi International Summer Schools*; Scoles, G., Ed.; Elsevier Science: Amsterdam, 1990.
(3) *Elemental and Molecular Clusters*; Benedek, G., Martin, T. P., Pacchioni, G., Ed.; Springer-Verlag: Berlin, 1988.
(4) *Structure and Dynamics of Weakly Bound Molecular Complexes*; Weber, A., Ed.; Reidel: Dordrecht, 1987.
(5) *Atomic and Molecular Clusters*; Bernstein, E., Ed.; Elsevier: Amsterdam, 1990.
(6) *Dynamics of Polyatomic van der Waals Complexes*; Halberstadt, N., Janda, K. C., Ed.; Plenum: New York, 1990.
(7) Castleman, A. W.; Keesee, R. G. *Acc. Chem. Phys.* **1986**, *19*, 413.
(8) Naaman, R. *Adv. Chem. Phys.* **1988**, *70*, 181.
(9) Janda, K. C. *Adv. Chem. Phys.* **1985**, *60*, 201.
(10) Alimi, R.; Gerber, R. B. *Phys. Rev. Lett.* **1990**, *64*, 1453.
(11) Garcia-Vela, A.; Gerber, R. B.; Valentini, J. J. *J. Chem. Phys.* **1992**, *97*, 3297.
(12) Goyal, S.; Schutt, D. L.; Scoles, G. *Acc. Chem. Res.* **1993**, *26*, 123.
(13) Hu, X.-C.; Martens, C. C. *J. Chem. Phys.* **1992**, *97*, 8805.

(14) Hu, X.-C.; Hase, W. L. *Z. Phys. D* **1992**, *25*, 57.
(15) Hurwitz, Y.; Rudich, Y.; Naaman, R.; Gerber, R. B. *J. Chem. Phys.* **1993**, *98*, 2941.
(16) Potter, E. D.; Liu, Q.; Zewail, A. H. *Chem. Phys. Lett.* **1992**, *200*, 605.
(17) Schutz, M.; Wulfert, S.; Leutwyler, S. *Z. Phys. D* **1991**, *20*, 247.
(18) Shalev, E.; Jortner, J. *Chem. Phys. Lett.* **1991**, *178*, 31.
(19) Syage, J. A. In *Ultrafast Spectroscopy in Chemical Systems*; Simon, J. D., Ed.; Kluwer Academic Publishers: Dordrecht, in press.
(20) Zhao, X. G.; Tucker, S. C.; Truhlar, D. G. *J. Am. Chem. Soc.* **1991**, *113*, 826.
(21) Leutwyler, S.; Bosiger, J. *Faraday Discuss. Chem. Soc.* **1988**, *86*, 225.
(22) Alexander, M. L.; Levinger, N. E.; Johnson, M. A.; Ray, D.; Lineberger, W. C. *J. Chem. Phys.* **1988**, *88*, 6200.
(23) Amar, F. G.; Berne, B. J. *J. Phys. Chem.* **1984**, *88*, 6720.
(24) Burke, M. L.; Klemperer, W. *J. Chem. Phys.* **1993**, *98*, 1797.
(25) Fei, S.; Zheng, X.; Heaven, C.; Tellinghuisen, J. *J. Chem. Phys.* **1992**, *97*, 6057.
(26) Hu, X.-C.; Hase, W. L. *J. Phys. Chem.* **1992**, *96*, 7535.
(27) Noorbatcha, I.; Raff, L. M.; Thompson, D. L. *J. Chem. Phys.* **1984**, *81*, 5658.
(28) Otto, B.; Schroeder, J.; Troe, J. *J. Chem. Phys.* **1984**, *81*, 202.
(29) Papanikolas, J. M.; Gord, J. R.; Levinger, N. E.; Ray, D.; Vorsa, V.; Lineberger, W. C. *J. Phys. Chem.* **1991**, *95*, 8028.
(30) Papanikolas, J. M.; Vorsa, V.; Nadal, M. E.; Campagnola, P. J.; Gord, J. R.; Lineberger, W. C. *J. Chem. Phys.* **1992**, *97*, 7002.
(31) Ray, D.; Levinger, N. E.; Papanikolas, J. M.; Lineberger, W. C. *J. Chem. Phys.* **1989**, *91*, 6533.
(32) Valentini, J. J.; Cross, J. B. *J. Chem. Phys.* **1982**, *77*, 572.
(33) Beck, T. L.; Berry, R. S. *J. Chem. Phys.* **1988**, *88*, 3910.
(34) Berry, R. S.; Beck, T. L.; Davis, H. L.; Jellinek, J. *Adv. Chem. Phys.* **1988**, *70*, 75.
(35) Berry, R. S. *J. Chem. Soc., Faraday Trans.* **1990**, *86*, 2343.
(36) Bosinger, J.; Leutwyler, S. *Phys. Rev. Lett.* **1987**, *59*, 1985.
(37) Bixon, M.; Jortner, J. *J. Chem. Phys.* **1989**, *91*, 1631.
(38) Cheng, H.-P.; Li, X.; Whetten, R. L.; Berry, R. S. *Phys. Rev. A* **1992**, *46*, 791.
(39) Hahn, M. Y.; Whetten, R. L. *Phys. Rev. Lett.* **1988**, *61*, 1190.
(40) Jellinek, J.; Beck, T. L.; Berry, R. S. *J. Chem. Phys.* **1986**, *84*, 2783.
(41) Kmetic, M. A.; Le Roy, R. J. *J. Chem. Phys.* **1991**, *95*, 6271.
(42) Leutwyler, S.; Furlan, A.; Knochenmuss, R.; Schutz, M.; Troxler, T.; Wulfert, S. *Z. Phys. D* **1991**, *20*, 209.
(43) Torchet, G. *Z. Phys. D* **1991**, *20*, 251.
(44) Farges, J.; de Faraudy, M. F.; Raoult, B.; Torchet, G. *J. Chem. Phys.* **1973**, *59*, 3454.
(45) Farges, J.; de Faraudy, M. F.; Raoult, B.; Torchet, G. *J. Chem. Phys.* **1986**, *84*, 3491.
(46) Wales, D. J.; Berry, R. S. *J. Chem. Phys* **1990**, *92*, 4283.
(47) Adams, J. E.; Stratt, R. M. *J. Chem. Phys.* **1990**, *93*, 1358.
(48) Beck, T. L.; Marchioro II, T. L. *J. Chem. Phys.* **1990**, *93*, 1347.
(49) de Pujo, P.; Mestdagh, J.-M.; Visticot, J.-P.; Cuvellier, J.; Meynadier, P.; Sublemontier, O.; Lallement, A.; Berlande, J. *Z. Phys. D.* **1993**, *25*, 357.
(50) Martens, C. C. *Phys. Rev. A* **1992**, *45*, 6914.
(51) Adams, J. E.; Stratt, R. M. *J. Chem. Phys.* **1990**, *93*, 1632.
(52) Cuvellier, J.; Mestdagh, J. M.; Meynadier, P.; de Pujo, P.; Sublemontier, O.; Visticot, J. P.; Berlande, J. *Chem. Phys. Lett.* **1991**, *176*, 325.
(53) Finney, L. M.; Martens, C. C. *J. Phys. Chem.* **1992**, *96*, 10626.
(54) Garcia-Vela, A.; Gerber, R. B.; Valentini, J. J. *Chem. Phys. Lett.* **1991**, *186*, 223.
(55) Honma, K.; Kajimoto, O. *J. Chem. Phys.* **1984**, *81*, 3344.
(56) Hu, X.-C.; Martens, C. C. *J. Chem. Phys.* **1993**, *98*, 8551.
(57) Hu, X.; Hase, W. L. *J. Chem. Phys.* **1993**, *98*, 7826.
(58) Kaukonen, H.-P.; Landman, U.; Cleveland, C. L. *J. Chem. Phys.* **1991**, *95*, 4997.
(59) Koehler, J.; Deal, R. M.; Hase, W. L.; Lu, D. *J. Cluster Sci.* **1990**, *1*, 335.
(60) Lallement, A.; Cuvellier, J.; Mestdagh, J. M.; Meynadier, P.; de Pujo, P.; Sublemontier, O.; Visticot, J. P.; Berlande, J.; Biquard, X. *Chem. Phys. Lett.* **1992**, *189*, 182.
(61) Nieman, J.; Naaman, R. *Chem. Phys.* **1984**, *90*, 407.
(62) Nieman, J.; Shwartz, J.; Naaman, R. *Z. Phys. D* **1986**, *1*, 231.
(63) Nieman, J.; Naaman, R. *J. Chem. Phys.* **1986**, *84*, 3825.
(64) Shin, S. K.; Chen, Y.; Nickolaisen, S.; Sharpe, S. W.; Beaudet, R. A.; Wittig, C. *Adv. Photochem.* **1991**, *16*, 249.
(65) Tardiff, J.; Deal, R. M.; Hase, W. L.; Lu, D. *J. Cluster Chem.* **1990**, *1*, 335.
(66) Visticot, J. P.; Mestdagh, J. M.; Alcaraz, C.; Cuvellier, J.; Berlande, J. *J. Chem. Phys.* **1988**, *88*, 3081.
(67) Wittig, C.; Sharpe, S.; Beaudet, R. A. *Acc. Chem. Res.* **1988**, *21*, 341.
(68) *Large Finite System*; Jortner, J., Pullman, A., Pullman, B., Eds.; D. Reidel: Dordrecht, 1987.
(69) Jortner, J. *Z. Phys. D* **1992**, *24*, 247.
(70) Jortner, J.; Even, U.; Ben-Horin, N.; Scharf, D.; et al. *Z. Phys. D* **1989**, *12*, 167.
(71) Hoare, M. R. *Adv. Chem. Phys.* **1979**, *40*, 49.
(72) Farges, J.; de Faraudy, M. F.; Raoult, B.; Torchet, G. *J. Chem. Phys.* **1983**, *78*, 5067.
(73) Farges, J.; de Faraudy, M. F.; Raoult, B.; Torchet, G. In *Large Finite Systems*; Jortner, J., Pullman, A., Pullman, B., Eds.; Reidel: Dordrecht, 1987; p 113.
(74) Torchet, G.; Farges, J.; de Feraudy, M. F.; Raoult, B. In *The Chemistry Physics of Atomic and Molecular Clusters. Proceedings of the International School of Physics "Enrico Fermi", Course CVII*; Scoles, G., Ed.; North Holland: Amsterdam, 1990; p 513.
(75) Berry, R. S. *Z. Phys. D* **1989**, *12*, 161.
(76) Berry, R. S. In *Large Finite Systems*; Jortner, J., Pullman, A., Pullman, B., Eds.; Reidel: Dordrecht, 1987; p 135.
(77) Goyal, S.; Robinson, G. N.; Schutt, D. L.; Scoles, G. *J. Phys. Chem.* **1991**, *95*, 4186.
(78) Jortner, J.; Ben-Horin, N. *J. Chem. Phys.* **1993**, *98*, 9346.
(79) Jortner, J.; Levine, R. D.; Rice, S. A. *Adv. Chem. Phys.* **1988**, *70*, 1.
(80) Perera, L.; Amar, G. *J. Chem. Phys.* **1989**, *90*, 7454.
(81) Amar, F. G.; Perera, L. *Z. Phys. D* **1991**, *20*, 173.
(82) Perera, L.; Amar, F. G. *J. Chem. Phys.* **1990**, *93*, 4884.
(83) Gough, T. E.; Mengel, M.; Rowntree, P. A.; Scoles, G. *J. Chem. Phys.* **1985**, *83*, 4958.
(84) Levandier, D. J.; McCombie, J.; Pursel, R.; Scoles, G. *J. Chem. Phys.* **1987**, *86*, 7239.
(85) Levandier, D. J.; Mengel, M.; Pursel, R.; McCombie, J.; Scoles, G. *Z. Phys. D—At., Mol. Clusters* **1988**, *10*, 337.
(86) Levandier, D. J.; Goyal, S.; McCombie, J.; Pate, B.; Scoles, G. *J. Chem. Soc., Faraday Trans.* **1990**, *86*, 2361.
(87) Crim, F. F. *Annu. Rev. Phys. Chem.* **1984**, *35*, 657.
(88) Crim, F. F. *Science* **1990**, *249*, 1387.
(89) Butler, L. J.; Ticich. T. M.; Likar, D. M.; Crim, F. F. *J. Chem. Phys.* **1986**, *85*, 2331.
(90) Ticich, T. M.; Rizzo, T. R.; Dubal, H.-R.; Crim, F. F. *J. Chem. Phys.* **1986**, *84*, 1508.
(91) Luo, X.; Rieger, P. T.; Perry, D. S.; Rizzo, T. R. *J. Chem. Phys.* **1988**, *89*, 4448.
(92) Luo, X.; Rizzo, T. R. *J. Chem. Phys.* **1990**, *93*, 8620.
(93) Scherer, N. F.; Doany, F. E.; Zewail, A. H.; Perry, J. W. *J. Chem. Phys.* **1986**, *84*, 1932.
(94) Scherer, N. F.; Zewail, A. H. *J. Chem. Phys.* **1987**, *87*, 97.
(95) Sumpter, B. G.; Thompson, D. L. *Chem. Phys. Lett.* **1988**, *153*, 243.
(96) Sumpter, B. G.; Thompson, D. L. *J. Chem. Phys.* **1985**, *82*, 4557.
(97) Sumpter, B. G.; Thompson, D. L. *J. Chem. Phys.* **1987**, *86*, 2805.
(98) Uzer, T.; Hynes, J. T.; Reinhardt, W. P. *Chem. Phys. Lett.* **1985**, *117*, 600.
(99) Uzer, T.; Hynes, J. T.; Reinhardt, W. P. *J. Chem. Phys.* **1986**, *85*, 5791.
(100) Uzer, T.; MacDonald, B. D.; Guan, Y.; Thompson, D. L. *Chem. Phys. Lett.* **1988**, *152*, 405.
(101) Getino, C.; Sumpter, B. G.; Santamaria, J.; Ezra, G. S. *J. Phys. Chem.* **1989**, *93*, 3877.
(102) Getino, C.; Sumpter, B. G.; Santamaria, J. *Chem. Phys.* **1990**, *145*, 1.
(103) Li, Y. S.; Whitnell, R. M.; Wilson, K. R.; Levine, R. D. *J. Phys. Chem.* **1993**, *97*, 3647.
(104) Gear, C. W. *SIAM J. Numer. Anal.* **1964**, *2B*, 69.